

PAPER • OPEN ACCESS

## Performance of Prototype of Optically Readout TPC with a $^{55}\text{Fe}$ source

To cite this article: I. Abritta Costa *et al* 2020 *J. Phys.: Conf. Ser.* **1498** 012017

View the [article online](#) for updates and enhancements.



**IOP | ebooks™**

Bringing together innovative digital publishing with leading authors from the global scientific community.

Start exploring the collection—download the first chapter of every title for free.

# Performance of Prototype of Optically Readout TPC with a $^{55}\text{Fe}$ source

I. Abritta Costa<sup>a</sup>, E. Baracchini<sup>b</sup>, F. Bellini<sup>a,c</sup>, L. Benussi<sup>d</sup>,  
S. Bianco<sup>d</sup>, M. Caponero<sup>d</sup>, G. Cavoto<sup>a,c</sup>, E. Di Marco<sup>a</sup>,  
G. Maccarrone<sup>d</sup>, M. Marafini<sup>e</sup>, G. Mazzitelli<sup>d</sup>, A. Messina<sup>a,c</sup>,  
D. Piccolo<sup>d</sup>, D. Pinci<sup>a</sup>, F. Renga<sup>a</sup>, F. Rosatelli<sup>d</sup>, G. Saviano<sup>d</sup> and  
S. Tomassini<sup>d</sup>

<sup>a</sup> Istituto Nazionale di Fisica Nucleare, Sezione di Roma, I-00185, Italy

<sup>b</sup> Gran Sasso Science Institute L'Aquila, I-67100, Italy

<sup>c</sup> Dipartimento di Fisica, Sapienza Università di Roma, I-00185, Italy

<sup>d</sup> Istituto Nazionale di Fisica Nucleare, Laboratori Nazionali di Frascati, I-00040, Italy

<sup>e</sup> Museo Storico della Fisica e Centro Studi e Ricerche "Enrico Fermi", Piazza del Viminale 1, Roma, I-00184, Italy

E-mail: emanuele.dimarco@roma1.infn.it

**Abstract.** The performances of an optical readout of Time Projection Chambers (TPCs) with multiple Gas Electron Multipliers (GEMs) amplification stages are presented. The detector is characterized by using  $^{55}\text{Fe}$  photons converting inside a 7 litre sensitive volume detector in different electric field configurations. This prototype is developed as part of the R&D for the CYGNO project for an application to direct Dark Matter search by detection of tracks of nuclear recoils in the gas within the keV energy range.

## 1. Experimental setup and data analysis

All measurements described in this work were carried out on a prototype for the future CYGNO experiment, called Large Elliptical MOdule (LEMON, Fig. 1) which is described in details in refs. [1, 2, 3].

The main elements of LEMON are:

- A sensitive volume (A) filled with 7 litres of He/CF<sub>4</sub> 60/40 gas mixture at atmospheric pressure, surrounded by a field cage (FC) composed of 20 elliptic silver plated wire rings with axes of 24 cm (along  $x$ ) and 20 cm (along  $y$ ) and a depth of 20 cm (along  $z$ ). The choice of an elliptical FC was driven by the optimisation of the coverage of the rectangular GEM planes;
- The sensitive volume is defined on one side by a semi-transparent cathode made of a thin wire mesh and on the other side by a structure of three 20×24 cm<sup>2</sup>, 50 μm thick GEMs;
- The whole structure is contained in a gas-tight box with two transparent windows on the cathode and the GEM sides;
- On the cathode side, beyond the window, a fast photo-multiplier tube (PMT) (B) is placed to read out as much as possible of the light produced by the GEMs;



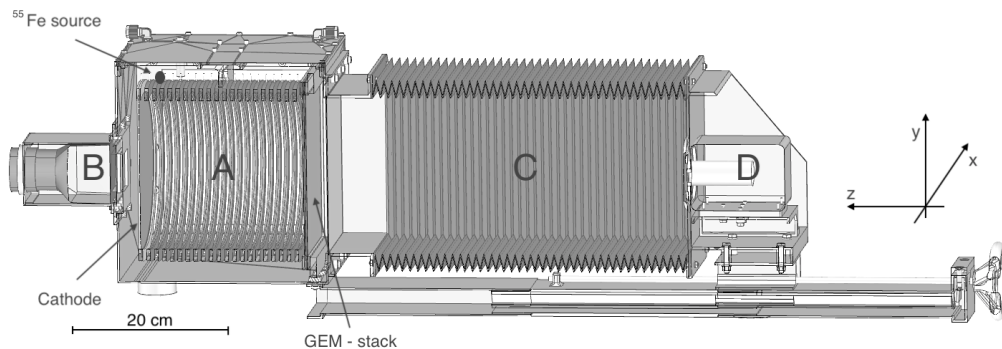


**Figure 1.** Drawing of the experimental setup. In particular, the elliptical field cage (A) close on one side by a triple-GEM structure and on the other side by a semitransparent cathode, the PMT (B), the adaptable bellow (C) and the CMOS camera with its lens (D) are visible.

- On the other side, downstream to an adjustable bellow (C), an ORCA Flash 4.0 camera,  $1.33 \times 1.33 \text{ cm}^2$  scientific CMOS sensor (subdivided in  $2048 \times 2048$  pixels with an active area of  $6.5 \times 6.5 \mu\text{m}^2$  each) and equipped with a Schneider lens distance of 52.5 cm (i.e. 21 Focal Length, FL) for the focalisation of the light produced in the GEM holes. In this configuration, the sensor is exposed to an effective surface of  $26 \times 26 \text{ cm}^2$  and therefore each pixel at an area of  $130 \times 130 \mu\text{m}^2$ . The geometrical acceptance therefore results to be  $1.6 \times 10^{-4}$  [4].

An  $^{55}\text{Fe}$  source, with an activity of about 100 Bq, was placed between two FC rings, 18 cm far from the top GEM as shown in Fig. 1. Because of the short distance between the plastic rings supporting the FC wires and their width along the  $x$  and  $y$  directions, these acted as a collimator for the photons emitted by the source, so that the effective distance from the GEMs of their interactions with the gas molecules was estimated to be  $18 \pm 2 \text{ cm}$ . Electrons produced within the sensitive volume are drifted by the electric field ( $E_d$ ), towards the GEMs where the multiplication process takes place. Typical operating conditions of the detector are:  $E_d = 600 \text{ V/cm}$ , an electric field in the GEM produced by  $\Delta V_{\text{GEM}} = 460 \text{ V}$  for each GEM plane (also referred as  $V_{\text{GEM}}$  in the figures) and a transfer field  $E_t = 2 \text{ kV/cm}$ . The maximum value of ( $E_d$ ) is limited by the maximum voltage provided by the HV generator (15 kV) used for the measurements reported in this paper.

The results presented are based on data acquired by the ORCA sensor in free running mode, without any trigger. The light produced during the multiplication process in the GEM were recorded during 100 ms exposures. The analysis algorithm is based on two steps:

- Pedestal subtraction: a blind run of 100 images was acquired with the sensor of the camera covered with its cap to cut out the ambient light. For each pixel, the pedestal is evaluated as the average number of counts recorded in this run and is subtracted to the counts collected in all recorded images. A sensor noise of 1.9 photons per pixel was measured as RMS of the pedestal distribution.
- Clustering: a very simple nearest neighbor-cluster (NNC) clustering algorithm was developed. A lower resolution version of each image was created with macro-pixels, defined as matrices of  $4 \times 4$  pixels. The average count over the 16 pixels, after subtracting their pedestal values, is assigned to each macro-pixel. A cluster is reconstructed by at least two neighbouring macro-pixels having more than 2 counts (i.e. 2 photons [5]) each.

Figure 2 shows an example of an image of two light spots due the interaction of  $^{55}\text{Fe}$  photons in the gas.

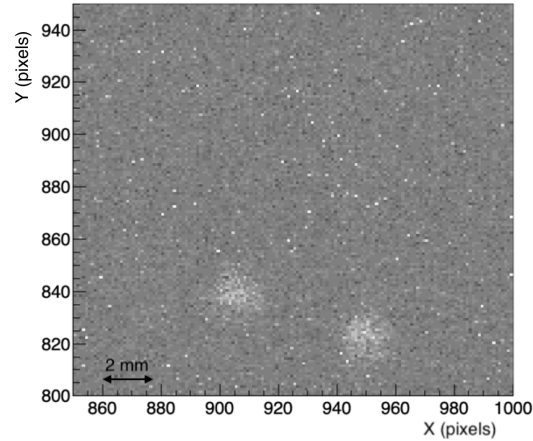


**Figure 2.** Example of two clusters due to X-ray interaction in gas.

## 2. Backgrounds

The CMOS sensor used for the measurements has two main sources of noise:

- a dark current of about 0.06 electrons per second per pixel;
- a readout noise of about 1.4 electrons RMS (in our set-up it was found to be slightly larger probably due to an effect of ageing of the sensor built more than 5 years ago);

The sensor electronic noise represents a possible unavoidable instrumental background and it can generate ghost-clusters (clusters including pixels not corresponding to energy deposits by particles). The distribution of the light in each ghost-cluster found in the blind run is shown in Fig. 3 (left).

The shape of the distribution is determined by the positively-definite counts of photons in the cluster. Its shape is used to estimate an operative threshold that allows to suppress fake signals due to sensor noise. The distribution is fitted with an exponential function:

$$p(L) = A_0 e^{-\frac{L}{\lambda}} \quad (1)$$

where  $L$  is the number of photons collected in the cluster. From the fitted parameters of this function, and by taking into account that a run lasts 10 s, it is possible to extrapolate the probability of having a ghost-clusters with an amount of light larger than a given threshold. As an example, a threshold of 300 photon counts corresponds to  $1 \times 10^{-4}$  ghost-clusters/second.

The GEM structure can, in principle, create a diffused light background because of possible micro-discharges. To evaluate it, the distribution of the light in the clusters reconstructed outside the sensitive area was studied. As it is shown in Fig. 3 (right), the obtained distribution is similar to the one due to the sensor electronic noise and has a tail that can be described with an exponential with a slope which is very similar to the one obtained for the sensor noise. The few events found outside the bulk of the distribution are short tracks very likely due to events that occurred close to the GEM, where the residual electric field of the GEM is able to capture electrons and drive them toward the multiplication channels.

As already described in Sec. 1, within the FC area an evident diffused and flat background is visible. To study it, a run without the radioactive source was acquired. Superimposing

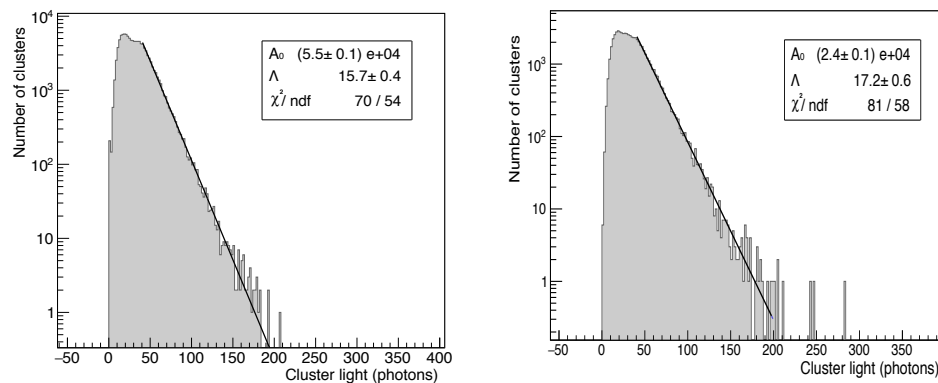


**Figure 3.** Left: Distribution of the light in clusters reconstructed in a run with blind sensor. Right: distribution of the light recorded clusters reconstructed outside from the sensitive area in a run with  $^{55}\text{Fe}$  source with superimposed exponential fit.

the images of all the reconstructed clusters in the whole run, results into an observed spatial distribution of clusters similar to the one found in presence of the source.

Figure 4 shows 10 overlapped events randomly chosen within the run. They appear as to

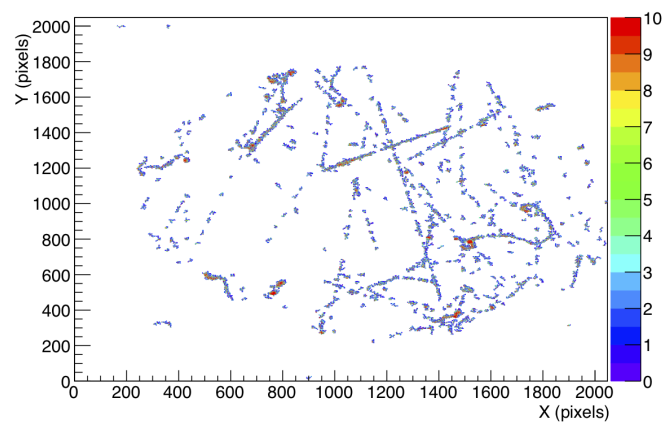


**Figure 4.** Example of 10 events acquired in a run without the  $^{55}\text{Fe}$  source within the detectors. Color scale indicates the number of photons collected per pixel.

be mostly tracks due to cosmic rays or low energy electrons from natural radioactivity. In a radio-pure apparatus operating underground such a background is expected to be strongly suppressed. Moreover, pattern recognition should be able to identify and reject residual events. For this reason, the effect of this background is not taken into account in this paper for the evaluation of the possible operative threshold.

### 3. Cluster size and light spectrum

For each run, the spectrum of the total light in clusters reconstructed within the sensitive area and the distribution of their size (i.e. the number of over threshold pixels) are studied. Figure 5 shows an example of these distributions for a run taken with  $\Delta V_{\text{GEM}} = 450$  V,  $E_d = 600$  V/cm and  $E_t = 2$  kV/cm.

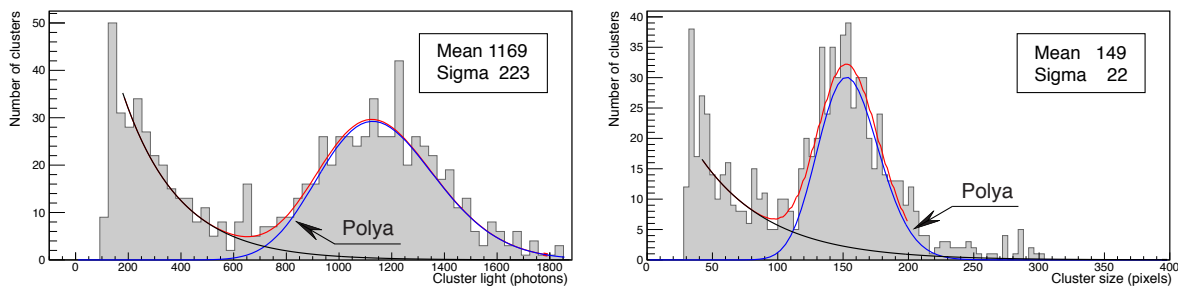


**Figure 5.** Distribution of total light (left) and number of illuminated pixels (right) for a run taken with  $\Delta V_{\text{GEM}} = 450$  V,  $E_d = 600$  V/cm and  $E_t = 2$  kV/cm.

Only clusters with at least 30 pixels over-threshold were considered. The distribution is fitted with the sum of an exponential function to model the background due to natural radioactivity (Sec. 2), and a Polya function, expressed by Eq. 2, often used to describe the response of MPGD to single-electron avalanche [6]:

$$P(n) = \frac{1}{b\bar{n}} \frac{1}{k!} \left( \frac{n}{b\bar{n}} \right)^k \cdot e^{-n/b\bar{n}} \quad (2)$$

where  $b$  is a free parameter and  $k = 1/b - 1$ . This function was found to describe the distribution of the signal better than a single Gaussian function in most of the voltage configuration, so it was preferred for its universality. The distribution has  $\bar{n}$  as expected value, while the variance is governed by its mean and the parameter  $b$ :  $\sigma^2 = \bar{n}(1 + b\bar{n})$ . From the result of the fits it is possible to evaluate:

- the expected value of the distribution  $\bar{n}$  and its variance  $\sigma^2$ . These parameters, when fitted on the light distributions, give the detector response in term of number of photons and the energy resolution (relative to the light response,  $\sigma/\mu$ ). When fitting the number of illuminated pixels distribution, the average size of the clusters can be evaluated by taking into account the effective area of  $130 \times 130 \mu\text{m}^2$  (see Sect. 1) acquired by each single pixel.
- the integral of the Polya component, that is proportional to the total number of reconstructed clusters and that can be used to evaluate the detection efficiency;

Since, as it is shown on the left of Fig. 5, in this configuration, on average  $1169 \pm 223$  photons are collected per cluster (i.e. each 5.9 keV released), a threshold of 400 photons corresponds to about 2 keV released in the sensitive volume. The average cluster size was found to be 149 pixels (Fig. 5, right).

#### 4. Results

The response of the detector to the  $^{55}\text{Fe}$  source has been studied as a function of three different operative parameters:  $\Delta V_{\text{GEM}}$ ,  $E_d$  and  $E_t$ . The results are reported in the following.

##### (i) Dependence on the voltage applied to the GEM ( $\Delta V_{\text{GEM}}$ )

The voltage applied to the GEM ( $\Delta V_{\text{GEM}}$ ) determines the gain and therefore the light yield of the structure. Then, the average number of collected photons per cluster and its fluctuations as a function of  $\Delta V_{\text{GEM}}$  is expected to raise at increasing  $\Delta V_{\text{GEM}}$ . Figure 6 (left) shows that the detector light yield increases exponentially and doubles every  $V_{\text{GEM}} = 30$  V step. The energy resolution is also found not to be significantly dependent

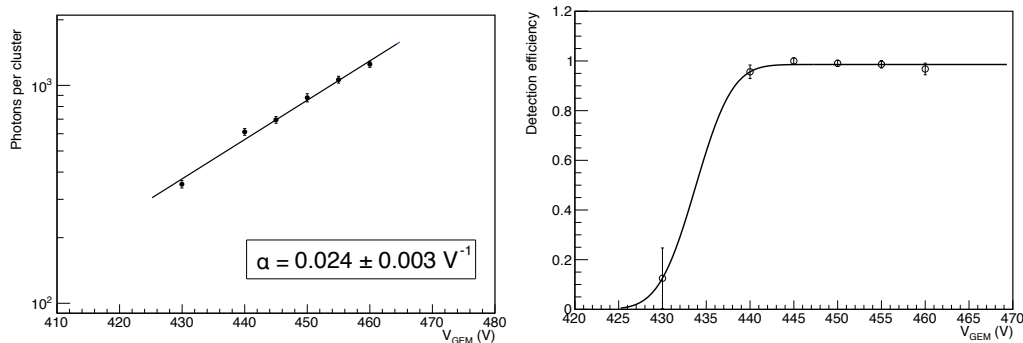


**Figure 6.** Left: average of the light spectrum with an exponential fit (left) as a function of  $\Delta V_{\text{GEM}}$  for a run taken with  $E_d = 600$  V/cm and  $E_t = 2$  kV/cm. Right: dimension spectra (right) and detection efficiency as a function of  $\Delta V_{\text{GEM}}$  for a run taken with  $E_d = 600$  V/cm and  $E_t = 2$  kV/cm.

on the voltage applied to the GEM with a value around 20% at 5.9 keV. Both results are found in good agreement with results obtained with a similar experimental setup [7].

The cluster size is also found to increase with the GEM voltage as the detector gets more efficient. On the right of Fig. 6, the total amount of the cluster detected normalised to its maximum value is shown. The lower edge of the plateau, at around  $V_{\text{GEM}} = 440$  V, is estimated as the minimal voltage to get the detector maximally efficient, with a global efficiency close to unity.

(ii) **Dependence on the Drift Field ( $E_d$ ):**

All measurements were taken with the  $^{55}\text{Fe}$  source 18 cm away from the readout plane and therefore, the response of the detector as a function of the electric field within the FC ( $E_d$ ) provides information on the effect of electron attachment and diffusion in our configuration.

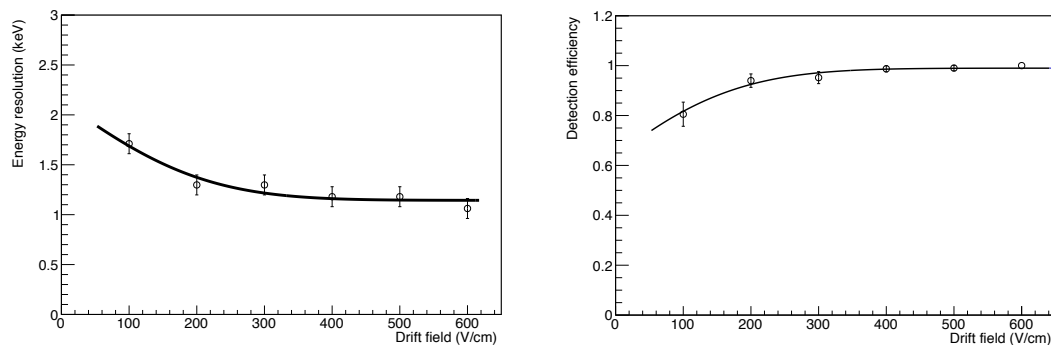


**Figure 7.** Left: Energy-equivalent resolution (left) and detection efficiency (right) as a function of  $E_d$  for a run taken with  $\Delta V_{\text{GEM}} = 450$  V and  $E_t = 2$  kV/cm.

Fluctuations of the number of photons per cluster (Fig. 7, left) have a small increase for small values of  $E_d$  (from around 20% to almost 30%). The detection efficiency (Fig. 7 right) remains well above 95% for  $E_d$  larger than 300 V/cm.

(iii) **Dependence on the Transfer Field ( $E_t$ )**

The electric field in the gap between the GEMs,  $E_t$ , plays a crucial role in the electron transport and on the effective gain of the detector. Because of a better capability in

extracting electrons [8], the number of collected photons increases linearly with the  $E_t$  reaching a value of 1200 for  $E_t = 2.5$  kV/cm (while their fluctuations are quite stable around 20%). In this configuration, therefore, a sensitivity of 0.2 collected photons per released keV was measured.

## 5. Conclusion

The analysis of the tests performed on the LEMON detector with 5.9 keV photons provided an important characterisation of its response. With a suitable field configuration ( $\Delta V_{\text{GEM}} = 460$  V,  $E_d = 600$  V/cm and  $E_t = 2.5$  kV/cm), the response of the detector is measured to be 1200 photon/cluster, i.e. 0.2 ph/eV. From the studies of the sensor intrinsic noise, it was possible to determine that a threshold of 400 photons ensures a rate of fake events smaller than 10 per year. With a sensitivity of 0.2 ph/eV this would represent a threshold of 2 keV. With an  $E_t = 2$  kV/cm, the detection efficiency was estimated to be well above 95% down to  $\Delta V_{\text{GEM}} = 430$  V where 1/3 of light is collected compared to  $\Delta V_{\text{GEM}} = 460$  V and  $E_t = 2.5$  kV/cm. Therefore, working with the latter settings would provide 3 more times light and thus, full detection efficiency seems possible for 2 keV signals.

## References

- [1] Antochi V C *et al.* 2017 *PoS EPS-HEP2017* 077
- [2] Antochi V C *et al.* 2017 *2017 IEEE Nuclear Science Symposium and Medical Imaging Conference (NSS/MIC)* pp 1–4 ISSN 2577-0829
- [3] Antochi V C *et al.* 2018 *2018 IEEE Nuclear Science Symposium and Medical Imaging Conference (NSS/MIC)* vol Under publication in IEEE Nuclear Science Symposium Medical Imaging Conference, 2018
- [4] Marafini M *et al.* 2018 *IEEE Transactions on Nuclear Science* **65** 604–608
- [5] Marafini M *et al.* 2015 *JINST* **10** P12010 (*Preprint 1508.07143*)
- [6] Blum W, Rolandi L and Riegler W 2008 *Particle detection with drift chambers* Particle Acceleration and Detection URL <http://www.springer.com/physics/elementary/book/978-3-540-76683-4>
- [7] Phan N S, Lee E R and Loomba D 2017 *arXiv 1703.09883* (*Preprint 1703.09883*)
- [8] Pinci D 2006 *A triple-GEM detector for the muon system of the LHCb experiment* Ph.D. thesis Cagliari University, CERN-THESIS-2006-070 URL <http://weblib.cern.ch/abstract?CERN-THESIS-2006-070>